Structure Development in Semicrystalline Diblock Copolymers Crystallizing from the Ordered Melt

A. J. Ryan,[†,‡] I. W. Hamley,[*,§] W. Bras,[‡,⊥] and F. S. Bates[∥]

Materials Science Centre, UMIST, Grosvenor Street, Manchester, M1 7HS U.K., DRAL Daresbury Laboratory, Warrington, Cheshire, WA4 4AD U.K., Department of Physics, University of Durham, South Road, Durham, DH1 3LE U.K., N.W.O., The Hague, The Netherlands, and Department of Chemical Engineering and Materials Science, University of Minnesota, Minneapolis, Minnesota 55455

Received January 9, 1995; Revised Manuscript Received March 13, 1995[⊗]

ABSTRACT: Time-resolved simultaneous synchrotron small-angle and wide-angle X-ray scattering (SAXS and WAXS) and DSC experiments have been performed on poly(ethylene)–poly(ethylethylene) and poly(ethylene)–poly(ethylene–propylene) diblock copolymers quenched from melts with lamellar and hexagonal-packed cylinder structures. We find that the original microphase-separated morphologies are destroyed due to poly(ethylene) (PE) chain folding upon crystallization. Below the melting temperature, a sample with a volume fraction $f_{PE} = 0.49$ forms a lamellar structure distinct from that in the melt. On quenching, a hexagonal $f_{PE} = 0.25$ sample forms a lamellar structure similar to that of the $f_{PE} = 0.49$ sample, while the hexagonal-packed cylinder structure of an $f_{PE} = 0.75$ sample is also destroyed by crystallization but does not form well-ordered lamellae. The SAXS profiles from crystallized materials are shown to correspond to the sum of scattering from block copolymer lamellae, with up to four orders of reflection, plus a broad peak arising from semicrystalline PE. Analysis of scattering density correlation functions calculated using the SAXS data shows that the PE lamellar thickness is (45 ± 5) Å for all samples, similar to that observed for PE homopolymer. The WAXS data reveal that PE crystallizes in its usual orthorhombic form in all samples. The relative degree of crystallinity as a function of time after a quench, determined from the SAXS invariant, is fitted by Avrami equations for spherulitic crystallite growth. The Avrami exponent is found to be $n = (3.0 \pm 0.1)$ for all samples, consistent with a nucleation and growth process.

Introduction

Structure formation in block copolymers continues to be of considerable experimental and theoretical interest.[1,2] A complete understanding of the phase behavior of even the simplest class of block copolymers—amorphous diblock copolymers—has yet to be achieved, as unanticipated new ordered phases have recently been observed near the order–disorder transition (ODT).[3–6]

The process of microphase separation that occurs in amorphous block copolymers results from segregation of incompatible components that are chemically linked. The resulting ordered structures thus have periods on the order of the polymer chain dimensions. In the simplest picture, lamellar, hexagonal-packed cylinder, or body-centered cubic phases are stable depending on the composition of the block copolymer.[7,8] The phase diagram of amorphous diblock copolymers, in the simplest mean field approximation,[7] is a function of f, the volume fraction of one component, and χN_t, where χ is the Flory–Huggins segmental interaction parameter (which is empirically found to be inversely proportional to temperature) and N_t is the total degree of polymerization. Close to the order–disorder transition ($\chi N_t \sim 10$) the blocks are weakly segregated with a nearly sinusoidal composition profile, while for $\chi N_t \gg 10$ they are strongly segregated.

In block copolymers containing a crystallizable component, structural changes, in particular chain folding, resulting from crystallization will compete with those occurring due to microphase separation. Previous experimental work[9–14] has demonstrated that the final morphology on crystallization depends on whether the sample is cooled from a microphase-separated state or crystallizes direct from the melt or solution. Cohen et al. studied a poly(styrene)–poly(ethylene/butene) (PS–PEB) diblock containing 11 wt % of the crystallizable PEB block that was solvent cast from toluene.[9] Crystallization within microphase-separated PEB spheres occurred when solvent casting was done above the PEB block melting temperature, T_m. When solvent was removed below T_m, crystallization did not occur within spherical microdomains; instead TEM and SANS experiments suggested an irregular structure. Séguéla and Prud'homme investigated a poly(ethylene)–poly(ethylene-*alt*-propylene)–poly(ethylene) (PE–PE/P–PE) triblock copolymer containing 27 wt % poly(ethylene) solvent cast above and below the poly(ethylene) T_m.[10] The samples cast above T_m crystallized within the assumed hexagonal-packed cylinder microphase-separated structure. However, small-angle X-ray scattering (SAXS), wide-angle X-ray scattering (WAXS), and tensile strain experiments performed on the samples cast at room temperature suggested that crystallization occurred without microphase separation.

Chain folding in poly(ethylene/butylene)–poly(ethylethylene) semicrystalline diblock copolymers was recently investigated using SAXS and WAXS on oriented specimens.[11] Microphase separation preceded crystallization for all samples, with 37–90 wt % poly(ethylene/butylene). From an analysis of pole figures for the (200) and (020) wide-angle reflections in two lamellar samples, the crystalline unit cell orientation was deduced, and it was found that the PEB chains are parallel to the layers.

The crystallization of poly(ϵ-caprolactone) in poly(ϵ-caprolactone)–poly(butadiene) diblock copolymers was

* To whom correspondence should be addressed.
† Materials Science Centre, UMIST.
‡ DRAL Daresbury Laboratory.
§ Department of Physics, University of Durham.
⊥ N.W.O.
∥ Department of Chemical Engineering and Materials Science, University of Minnesota.
⊗ Abstract published in *Advance ACS Abstracts,* April 15, 1995.

0024-9297/95/2228-3860$09.00/0

investigated using time-resolved SAXS by Nojima et al.[13] A sample with an order–disorder temperature $T_{ODT} < T_m$ quenched directly from the homogeneous melt did not show the sharp diffraction peaks characterizing a microphase-separated phase; i.e., crystallization proceeded directly. However, for two samples with $T_{ODT} \sim T_m$ quenched from the homogeneous melt, microphase separation preceded crystallization, as evidenced by the appearance of transient sharp diffraction peaks in the SAXS curves. The ordered melt morphology was destroyed by crystallization. An important factor in these observations could be the proximity of the T_m to the T_{ODT}, as noted by Rangarajan and co-workers.[14] They suggest that since crystallization occurs just below T_{ODT}, the energy barrier to disrupting the microphase-separated morphology can readily be overcome. We will investigate this issue in this work, where samples with T_{ODT} substantially greater than T_m are quenched from a microphase-separated melt. We also studied a sample with $T_{ODT} \sim T_m$.

The morphology of poly(ethylene)–poly(ethylene/propylene) (PE–PE/P) diblocks of various compositions quenched from the homogeneous melt below the poly(ethylene) melting point has recently been studied.[14] For all compositions (12–56 wt % poly(ethylene)), a lamellar morphology with a spherulitic superstructure was shown by SAXS and small-angle light scattering, respectively. This was interpreted to mean that crystallization was not influenced by microphase separation in this case, because asymmetric amorphous diblocks would not form lamellar structures. A model for the poly(ethylene) crystallite structure was also proposed where the poly(ethylene) chains are along the layer normals sandwiching a region of amorphous poly(ethylene), a structure similar to that of a semicrystalline homopolymer. The model was inferred from WAXS and DSC data which revealed that the poly(ethylene) degree of crystallinity was much less than 100%.

This work is concerned with the structure of poly(ethylene)–poly(ethylethylene) (PE–PEE) diblocks quenched from lamellar and hexagonal-packed cylinder microphase-separated phases below the poly(ethylene) crystallization temperature. We present time-resolved synchrotron SAXS and WAXS data for samples with poly(ethylene) volume fractions $f_{PE} = 0.25$, $f_{PE} = 0.49$, and $f_{PE} = 0.75$, thus spanning systems where poly(ethylene) is the matrix containing cylinders of PEE, where it is layered, and where it is confined in hexagonal-packed cylinders. We also briefly discuss SAXS/WAXS data for poly(ethylene)–poly(ethylene–propylene) diblocks. However, the SAXS data is rather featureless, and a detailed analysis of it is not possible. DSC was used to determine the PE degree of crystallinity in all samples.

This paper is organized as follows. In section 2 the sample synthesis and characterization are described together with details of the SAXS/WAXS and DSC experiments. In section 3 we first discuss the data for the structural changes resulting from crystallization before discussing the crystallization kinetics. Finally, we summarize our conclusions.

Experimental Section

A. Sample Synthesis and Characterization. Chemical structures of the PE–PEE and PE–PEP diblocks studied are shown in Figure 1. Full details of the polymer synthesis and characterization are given elsewhere.[15] Here we merely outline the general methods. The polyolefin diblocks were synthesized by catalytic hydrogenation or deuteration of

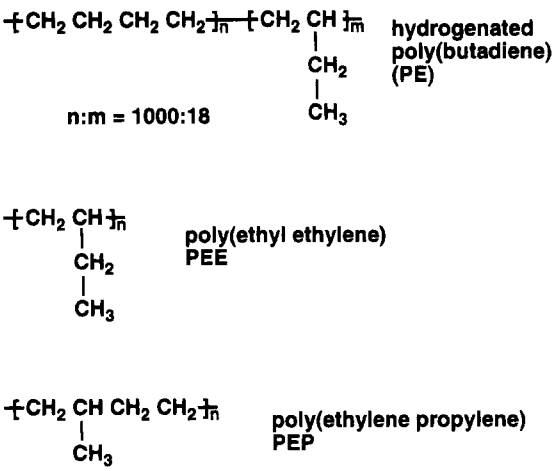

Figure 1. Chemical structures of hydrogenated polybutadiene, poly(ethylethylene), and poly(ethylene–propylene).

Table 1. Sample Characteristics

sample	f_{PE}	$10^{-3} M_n$/ g mol^{-1}	morphology	T_{ODT}/°C (T_{OOT}/°C)
PEP–PE-1D	0.50	80	lamellar	120
PEP–PE-3H	0.50	120	lamellar	159
PEP–PE-4D	0.24	153	hex/bcc	(130), 143
PEP–PE-10D	0.75	180	hexagonal	159
PE–PEE-2D	0.55	20	lamellar	$<T_m$
PE–PEE-3D	0.49	23	lamellar	121
PE–PEE-7H	0.75	44	hexagonal	148
PE–PEE-11D	0.25	47	hex/bcc	(238), 273

polydiene precursors, which were anionically polymerized from butadiene and isoprene monomers. The precursor for poly(ethylene) is poly(1,4-butadiene) (93% 1,4 and 7% 1,2 addition), that for poly(ethylethylene) is poly(1,2-butadiene) (>99% 1,2 addition), and that for poly(ethylene–propylene) is poly(1,4-isoprene) (95% 1,4 and 5% 3,4 addition). The indicated microstructures are typical for the reaction conditions employed.[16] Deuteration was performed to provide scattering contrast for neutron experiments, but is not required for synchrotron X-ray scattering.

The number-average molecular weights and compositions listed in Table 1 were determined from the synthesis stoichiometry, which has been found to be a reliable measure of the molecular weight. Weight-average molecular weights for selected polyolefin diblocks or diene precursors were determined using light scattering experiments. Molecular weight distributions were determined using size exclusion chromatography and were found to be narrow ($M_w/M_n < 1.1$). The samples have also been characterized using rheology. Selected rheology data for PE–PEE-7H is presented in ref 17, while that for PE–PEE-3D and PE–PEE-11D will be reported in ref 18.

The PE block in the PE–PEE and PE–PEP materials is composed of a random distribution of poly(ethylene) and poly(ethylethylene) repeat units with 18 ethyl branches per 1000 backbone carbon atoms. The microstructure leads to a reduction in the melting temperature, degree of crystallinity, and long period relative to high-density (linear) poly(ethylene). For the PE homopolymer $T_m = 108$ °C (fully protonated version) with roughly 40% crystallinity and a long period of 134 Å.

Differential scanning calorimetry (DSC) experiments were performed using a TA Instruments TA2000 DSC equipped with a 910 DSC head. Temperature and enthalpy values were calibrated using indium as a standard. Measurements were made on 10 mg samples sealed in aluminum pans on the first heating ramp.

B. Synchrotron X-ray Scattering. Simultaneous SAXS and WAXS experiments were performed on beamline 8.2 of the Synchrotron Radiation Source (SRS) at the Daresbury Laboratory, Warrington, U.K. Details of the storage ring, radiation, camera geometry, and data collection electronics

Table 2. DSC and SAXS/WAXS Results[a]

sample	T_m/°C	ΔH_f/J g^{-1}	X_{PE} (%) DSC	X_{PE} (%) SAXS	d' (l')/Å	d_{melt}/Å (n)	d_{sol}/Å (n)	transitions obsd
PE	108	113	39	31	134 (41)			C
PEP–PE-1D	105	64.8	44					C
PEP–PE-3H	104	60.4	41					C
PEP–PE-4D	100	32.0	45					C
PEP–PE-10D	103	60.4	28					C
PE–PEE-2D	106	63.5	39	30	154 (46)	209 (1)	314 (4)	ODT + C
PE–PEE-3D	106	67.3	47	31	153 (47)	224 (1)	314 (4)	ODT + C
PE–PEE-11D	103	35.9	39	31	138 (43)	349 (2)	449 (4)	C

[a] The PE melt temperature (T_m) and melting enthalpy (ΔH_f) are determined from DSC measurements. The PE degree of crystallinity, X_{PE}, is estimated from the DSC and SAXS data. The total PE domain thickness d' and crystalline region thickness l' have been determined from an analysis of the SAXS correlation function. The domain periods d are computed as $2\pi/q^*$, with q^* the position of the first-order peak. The number of peaks observed is denoted n, and crystallization and order–disorder transitions are denoted C and ODT, respectively.

have been given elsewhere.[19] White radiation from the source was monochromated using a cylindrically bent Ge(111) crystal to give an intense beam of $\lambda = (1.50 \pm 0.01)$ Å X-rays. With the SRS operating at 2 GeV and 200 mA, a flux of 4×10^{10} photons s^{-1} is generated at the sample position. The beam is highly collimated to a typical cross-section of 0.3×4 mm^2 in the focal plane.

The instrument is equipped with a multiwire quadrant detector for SAXS located 3.5 m from the sample position and a curved knife-edge WAXS detector that covers 120° of arc at a radius of 0.3 m. A vacuum chamber is placed between the sample and detectors to reduce air scattering and absorption. Both the exit window of the beam line and the entrance window of the vacuum chamber are made from 15 μm mica; the exit windows of the vacuum chambers are made from 15 μm mica and 10 μm Kapton film for the WAXS and SAXS detectors, respectively.

The WAXS detector has a spatial resolution of 50 μm and can be used up to 100 000 counts s^{-1}; only 90° of arc is active in these experiments, the rest of the detector being shielded with lead. The SAXS detector measures intensity in the radial direction (over an opening angle of 70° and an active length of 0.2 m) and is only suitable for isomorphous scatterers. The active area increases radially, improving the signal-to-noise ratio at larger angles compared to single-wire detectors. The spatial resolution of the SAXS detector is 500 μm and it can handle up to ~250 000 counts s^{-1}.

The samples for SAXS/WAXS were prepared by placing pieces of polymer cut from sheets in a cell comprising a DuPont DSC pan fitted with windows (≈4 mm diameter) made from 5 mm thick mica. Sealed pans were placed in a spring-loaded holder in a Linkam TMH600 hot stage mounted on an optical bench. The design and operation of the X-ray DSC have been described in detail elsewhere.[20] The silver heating block of the hot stage contains a 4×1 mm tapered slot which allows the transmitted and scattered X-rays to pass through unhindered. Variable heating rates were used, with a nominal cooling rate for quenches of 40 °C min^{-1}. Temperature drifts across the sample chamber necessitate direct measurement of the temperature at the sample position, in addition to the temperature monitoring and control of the furnace.

A scattering pattern from an oriented specimen of wet collagen (rat-tail tendon) was used to calibrate the SAXS detector, while HDPE, aluminum, and an NBS silicon standard were used to calibrate the WAXS detector. A parallel-plate ionization detector placed before the sample cell recorded the incident intensities. The experimental data were corrected for background scattering (from the camera, hot stage, and empty cell), sample absorption, and the positional alinearity of the detectors.

Results and Discussion

The DSC results given in Table 2 show that the degree of crystallinity of the poly(ethylene) in our samples is $X_{PE} = (40 \pm 10)\%$. The PE degree of crystallinity is estimated from the DSC data using $X_{PE} = \Delta H_{exp}/\Delta H_f^\circ w_{PE}$, where w_{PE} is the weight fraction of PE and $\Delta H_f^\circ = 277$ J g^{-1} is the theoretical heat of fusion for 100% crystalline PE.[21] The values of X_{PE} determined from the SAXS correlation function as l'/d' (here l' is the crystalline region thickness and d' is the total PE domain thickness) are in reasonable agreement, considering the approximate nature of the procedure used to determine layer thicknesses. The SAXS values are systematically lower than the DSC values because they are determined close to the crystallization temperature (at 95 or 100 °C). These values are comparable to those for PE (see Table 2).

We will not present further data for the PE–PEP samples because we found that the X-ray scattering contrast in these materials was insufficient to resolve peaks in the melt. The PE–PEE samples have higher contrast for X-rays so that simultaneous SAXS and WAXS data could be collected using 6 s frames for one pattern. The transitions observed in the SAXS/WAXS data are indicated in Table 2.

PE–PEE-2D crystallizes directly from the homogeneous melt (as shown in Figures 6 and 7). In the homogeneous disordered melt a single peak in the SAXS pattern arises from the correlation hole effect.[7] SAXS profiles obtained at different times at 95 °C are shown in Figure 2a. The transition from the melt to crystalline solid is shown by the development of four orders of Bragg peak. The second-order reflection is more intense than the first for this sample because the pattern contains contributions from a narrow distribution lamellar structure with $d \approx 314$ Å and from a broad distribution centered around $d \approx 150$ Å. The peak position of the first reflection, q^*, decreases discontinuously as crystallization occurs. This is because the poly(ethylene) chain folding leads to a large increase in the poly(ethylene) domain thickness.

SAXS data for PE–PEE-3D are presented in Figure 2b. After cooling from 140 °C where the sample is disordered (bottom curve) to 100 °C at 40 °C/min, a transition occurs from the disordered melt to an ordered melt, based on a discontinuous change in the intensity of the single scattering peak observed. Based on previous neutron scattering measurements, the microphase-separated phase is identified as lamellar.[18] In the crystalline solid, the intensity of the second-order peak is enhanced because the block copolymer reflections are superposed on a broad peak that comes from semicrystalline PE. This is similar to the SAXS pattern for PE–PEE-2D; indeed the second-order peak in PE–PEE-3D is more intense than the first order for a period during the crystallization process. We will return to a more detailed discussion of the origin of the crystalline solid scattering pattern and its kinetic development shortly. A major difference between PE–PEE-3D and PE–PEE-2D is that the equilibrium order–disorder transition for

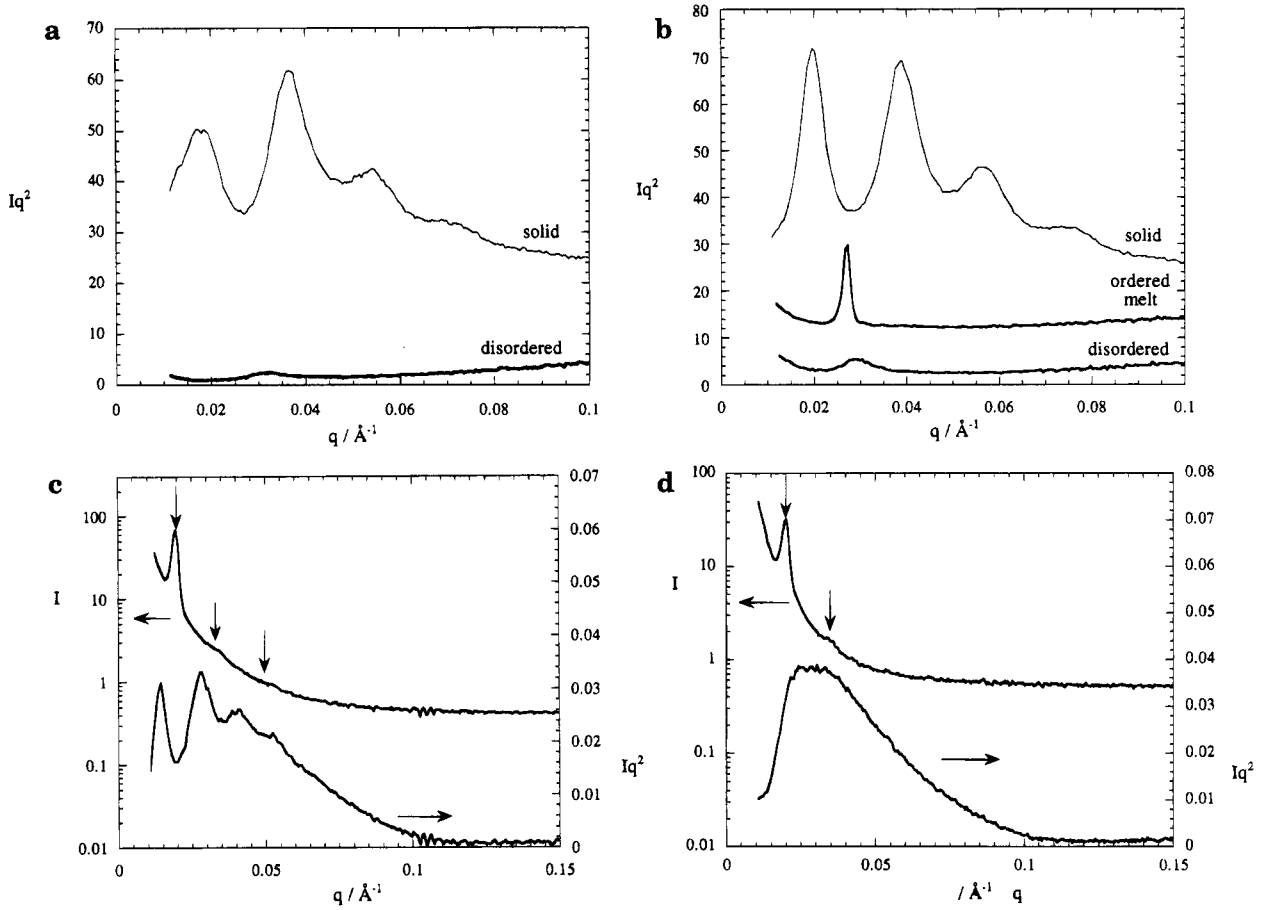

Figure 2. Lorentz-corrected SAXS intensity versus scattering vector magnitude for (a) PE–PEE-2D (both profiles at 95 °C), (b) PE–PEE-3H (top two profiles at 100 °C, bottom profile at 140 °C), (c) PE–PEE-11D (top, 140 °C; bottom, 100 °C), and (d) PE–PEE-7H (top, 140 °C; bottom, 100 °C).

the former occurs above the melting temperature, so that an ordered melt structure can be observed.

In contrast to the nearly symmetric PE–PEE diblocks, PE–PEE-11D with $f_{PE} = 0.25$ forms a hexagonal phase in the ordered melt, as evident from the location of the higher order reflections in the SAXS data at 140 °C shown in Figure 2c. Weak reflections are observed centered at q^*, $\sqrt{3}q^*$, and $\sqrt{7}q^*$. The $\sqrt{4}q^*$ reflection also allowed for a hexagonal cylinder structure is absent because there is a cylinder form factor minimum at this location for diblock compositions close to $f = 0.75$.[22] On cooling below the melting temperature, the ordered melt structure was destroyed, as shown by the data in Figure 2c at 100 °C. Four orders of reflection are observed at nq^*, n = 1,2,3,4, which is characteristic of a lamellar structure. The structural period $d = 2\pi/q^*$ has increased substantially compared to the ordered melt, as for the symmetric diblocks, and the Bragg peaks lie on the broad PE peak. This data provides clear evidence that crystallization into lamellae has overwhelmed microphase separation even when the microphase-separated phase is not lamellar.

The crystallization of an asymmetric diblock where poly(ethylene) is the minority component (PE–PEE-11D) may be contrasted with that for one where it is the majority component. SAXS data for such a sample, PE–PEE-7H with $f_{PE} = 0.75$, are presented in Figure 2d. The ordered melt is a hexagonal-packed cylinder phase, consistent with the observed reflections at q^* and $\sqrt{3}q^*$. Neutron scattering data confirm the identification of this morphology.[17] However, the SAXS pattern changes upon crystallization to a broad asymmetric

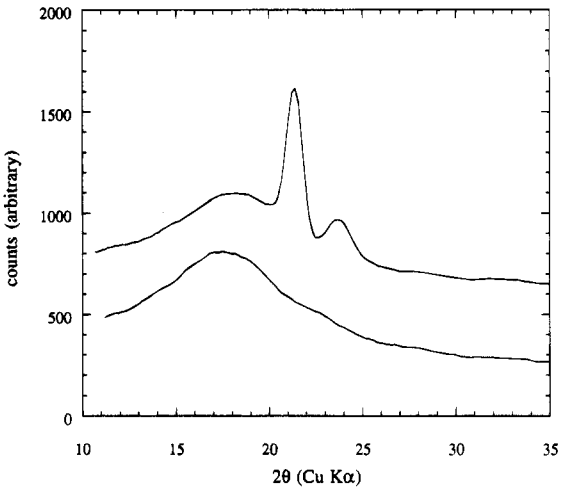

Figure 3. Wide-angle X-ray scattering intensity profile for PE–PEE-7H at 100 °C (top) and 140 °C (bottom).

peak, which is dominated by semicrystalline PE scattering. We are unable to unambiguously identify the morphology in the solid, although it is unlikely to be lamellar based on comparison with the SAXS profile for PE–PEE-11D.

A representative WAXS pattern is shown in Figure 3. Similar patterns were obtained for all samples. In the melt a broad peak which is scattering from amorphous poly(ethylene) is present. Upon crystallization, (110) and (200) Bragg reflections are observed superimposed on the amorphous peak. These Bragg reflections are those observed for poly(ethylene) homopolymer

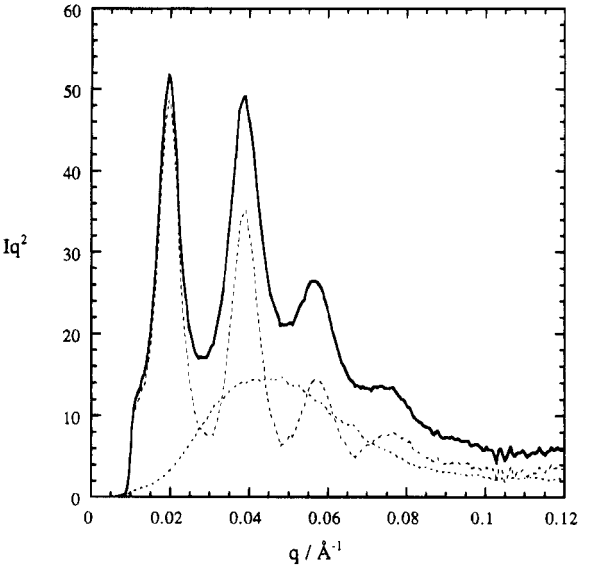

Figure 4. Plot showing that the SAXS intensity profile from PE−PEE-3D lamellae at a temperature below the PE crystallization temperature can be represented as the sum of a broad peak from amorphous and crystalline PE (dashed curve with one peak) plus the multiple Bragg peak scattering from a lamellar structure (dashed curve with four peaks).

and indicate that poly(ethylene) has crystallized in its usual orthorhombic form.[21]

The scattering from samples where crystallization has occurred can be considered to arise from a lamellar structure with a period $d_{sol} = d_{PE} + d_{PEE}$, where d_{PE} is the thickness of the PE domain and d_{PEE} is that of the PEE domain. This is illustrated for PE−PEE-3D in Figure 4. The PE domain consists of both amorphous and crystalline material which gives rise to a broad peak, typically centered near $q = 0.05$ Å^{-1}, as shown in the SAXS profile from a sample of PE in Figure 4. The intensities in this curve have been multiplied by $^1/_2$ to allow for the volume fraction of PE in PE−PEE-3D so that the curve can be subtracted from the measured profile for PE−PEE-3D. The difference curve is then the contribution from a single-period regular lamellar structure, and the intensity of the Bragg peaks at nq^* decreases smoothly as n increases.

Scattering density correlation functions were computed from the SAXS data, and the thickness of the crystalline poly(ethylene) region was determined from the extrapolated linear region of the scattering density correlation function using[23]

$$\gamma_1(r) = \frac{\int_0^\infty I(q)q^2 \cos(qr)\, dq}{\int_0^\infty I(q)q^2\, dq} \qquad (1)$$

which has been normalized such that $\gamma_1(r=0) = 1$. Here $q = 4\pi \sin\theta/\lambda$, where 2θ is the scattering angle and λ is the X-ray wavelength. The data was extrapolated to large q using a damped Porod function of the form

$$I(q) = k \exp(\sigma^2 q^2)/q^4 + I_b \qquad (2)$$

where I_b is a background. Extrapolation to low q was performed using an intensity profile based on Guinier's law. Further details of this procedure are given elsewhere.[24] The extrapolated slope of the linear region of the correlation function is related to the size of the smallest scattering domain in the system.[25]

Results of these calculations for our PE−PEE samples and PE are shown in Figure 5a. This immediately reveals qualitative differences between the structures of different samples. A detailed interpretation of the correlation function for PE−PEE-3D is illustrated in Figure 5b. The shortest distance in the structure is determined from the extrapolated slope of the linear region of $\gamma_1(r)$ and is within the range (45 ± 5) Å for all samples, including PE. This is the thickness of the PE domain because $X_{PE} < 0.5$. The location of the crystalline region within the PE domain cannot be deduced from our data, which is for a powder sample; consequently any information on orientation is lost. The model in Figure 5b is a one-dimensional model simply intended to show the domain thicknesses. However, we will show elsewhere that for oriented samples the scattering from the lamellar microstructure and that from the semicrystalline PE add incoherently, so that the contributions from each can simply be summed.[26] As discussed in the Introduction, there are conflicting reports on the orientation of the chain-folded PE. We will report on further experiments on oriented specimens in a forthcoming publication.[26] The weak maximum in $\gamma_1(r)$ near 150 Å appears to arise from the thickness d' of the amorphous + crystalline PE domain. For the samples which form lamellae, an additional peak in $\gamma_1(r)$ is observed with a position which matches closely that determined from $d_{sol} = 2\pi/q^*$. This is the total lamellar period in the structure. The correlation function for PE−PEE-7H differs qualitatively from the others because the pronounced maxima at $r \neq 0$ are absent. This supports our assertion that the structure is not lamellar with two periods. However, we cannot interpret the correlation function further as the procedure used to evaluate it is not valid for nonlamellar structures.

We present the computed small-angle scattering invariant for several polymers. The small-angle scattering invariant is a measure of the total small-angle scattering from a material, independent of the size or shape of structural inhomogeneities.[27] In our samples, it is proportional to the degree of crystallinity because the electron density increases in the crystalline regions. It is then given by[28]

$$Q = \phi(1-\phi)\langle\eta^2\rangle = \frac{1}{2\pi i_e}\int_0^\infty I(q)q^2\, dq \qquad (3)$$

where ϕ is the volume fraction of crystallites, η is the electron density difference between the crystalline and amorphous phases, and i_e is the Thompson scattering factor. The absolute value of the invariant requires absolute intensity measurements, thermal background subtraction, and extrapolation to $q = 0$ and $q = \infty$ and is computationally difficult to achieve. Therefore we instead calculate a relative invariant Q' from the area under the $I'q^2$ curve between the first data point at $q = 0.01$ Å^{-1} and the region in which $I(q)q^2$ becomes constant (at $q = 0.20$ Å^{-1}). Here I' is the measured intensity minus a flat background contribution. The relative degree of crystallinity can then be computed using eq 3.

Analogously to the relative SAXS invariant, the degree of crystallinity can be computed by assuming that the scattering within a certain region of reciprocal space is independent of the state of aggregation of the polymer. Then the relative degree of crystallinity can be found from the ratio of the integrated intensity of the crystal peak to that of the total amorphous and

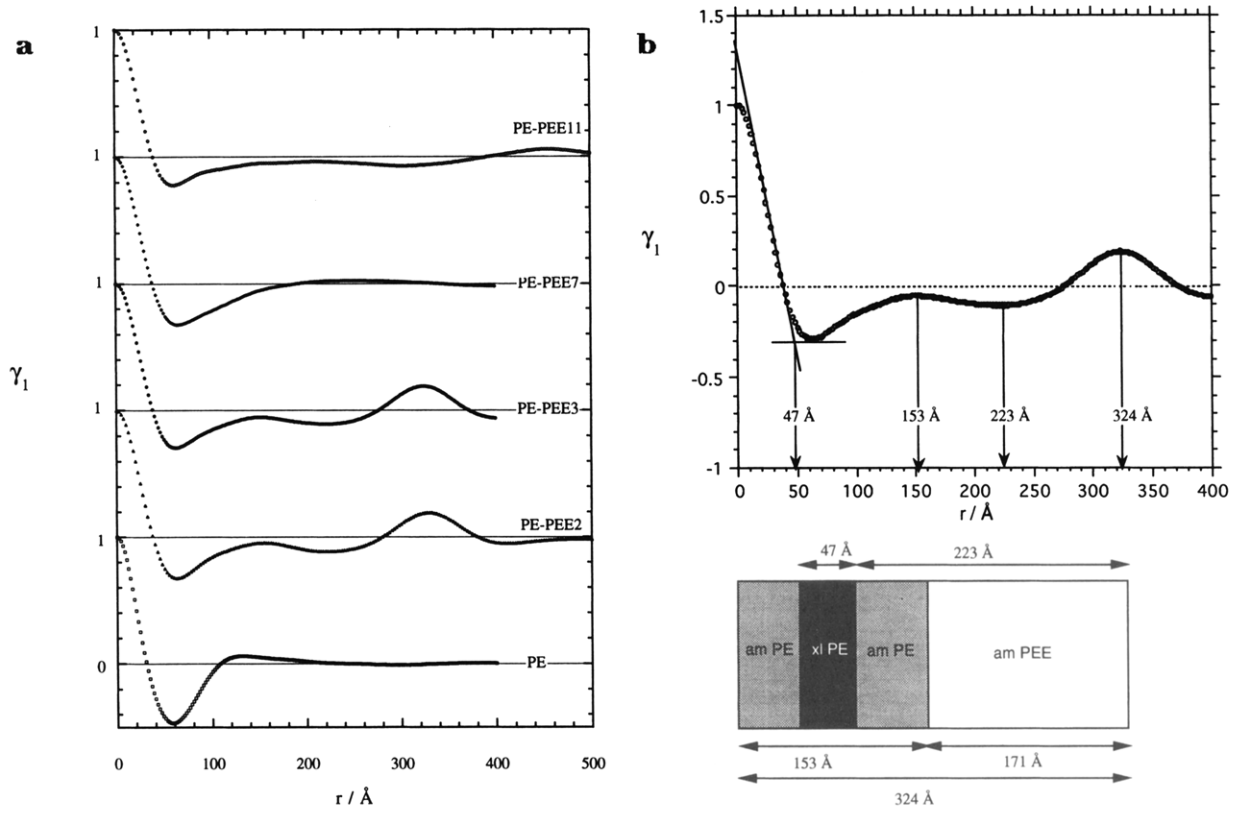

Figure 5. (a) Cosine-transform correlation functions computed from the SAXS data for PE-containing diblocks and PE. (b) Interpretation of the correlation function for PE−PEE-3D, based on the distances determined from extrapolation of the small r slope and subsequent peak maxima and minima.

crystalline scattering,[27]

$$X_{PE} = \frac{I_c}{I_c + I_a} \tag{4}$$

where I_c and I_a are respectively the integrated intensities of the crystalline and amorphous components of the scattering. For PE the amorphous scattering below the (110) peak is relatively insensitive to the degree of crystallinity so a simple integration of the (110) reflection is directly proportional to X_{PE} (however, we cannot determine absolute values in this way).

The time evolution of the SAXS profile for PE−PEE-2D during a quench from 140 to 100 °C is shown in Figure 6. The temperature reached 100 °C at 60 s, at which time the sample was still disordered. After 120 s the sample crystallizes as revealed in the SAXS by the development of four orders of Bragg peaks, with a domain spacing $d_{sol} = 2\pi/q^*$ much larger than that for the melt (see Table 2). Figure 7 contrasts the crystallization of PE−PEE-2D with that of PE−PEE-3D. For the former, crystallization occurs directly from the disordered melt, as shown by the simultaneous sharp increase of the intensity of the most intense peak and the SAXS invariant following a quench to a representative temperature of 100 °C. In contrast, the intensity at q^* for PE−PEE-3D increases sharply before the invariant, signaling a disorder−order transition in the melt prior to crystallization.

The kinetics of crystallization of PE−PEE-3D at 95 °C following rapid cooling from 140 °C are illustrated by the SAXS profiles in Figure 8. The melt disorder−order transition is readily apparent at 60 s and is followed by crystallization at 162 s. The ordered melt structure in this sample is in equilibrium in the interval

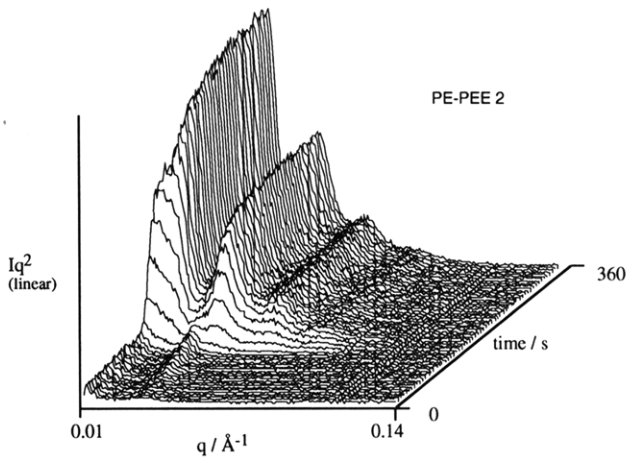

Figure 6. SAXS patterns for PE−PEE-2D during a temperature quench from 140 to 100 °C at 40 °C/min and then holding at 100 °C.

from 106 to 121 °C, as confirmed by its observation on heating and cooling. There appears to be a short biphasic region as the ordered melt crystallizes. It may also be observed that after the initial stage of PE crystallization the Bragg reflections develop in intensity at a similar rate, consistent with a nucleation and growth process. This is confirmed by an Avrami analysis of the crystallization kinetics of the whole SAXS pattern that is discussed shortly. During the crystallization process the second-order peak is transiently more intense than the first order. We will return to this when discussing Figure 11. In contrast to the crystallization process, for most undercoolings the kinetics of the order−disorder transition in the melt will be governed by the rate of heat transfer.[29]

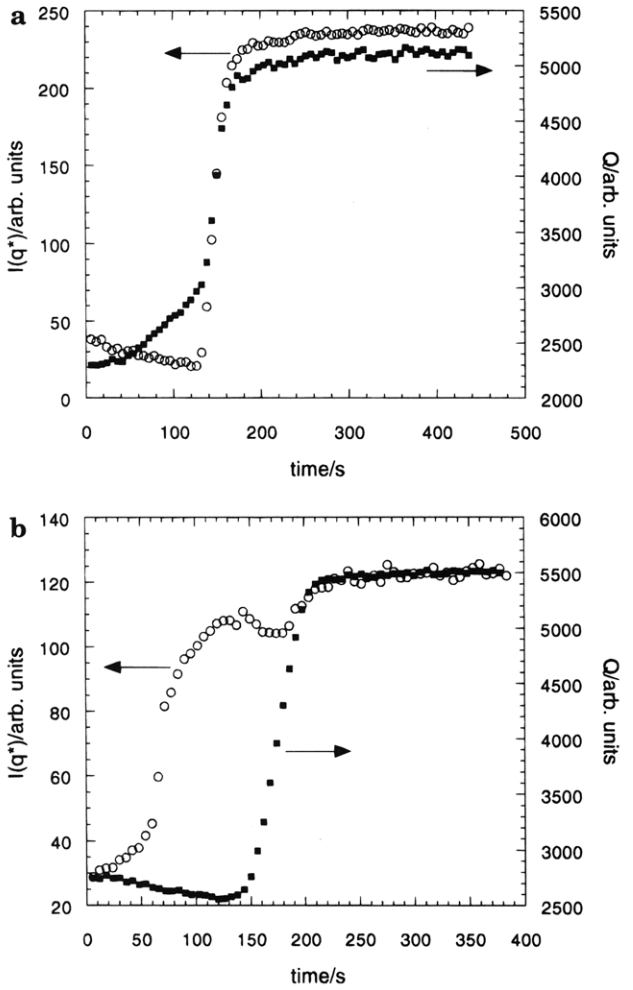

Figure 7. Variation of the intensity of the most intense peak (open circles) and of the SAXS invariant (filled squares) following a quench from 140 to 95 °C. (a) PE−PEE-2D; (b) PE−PEE-3D.

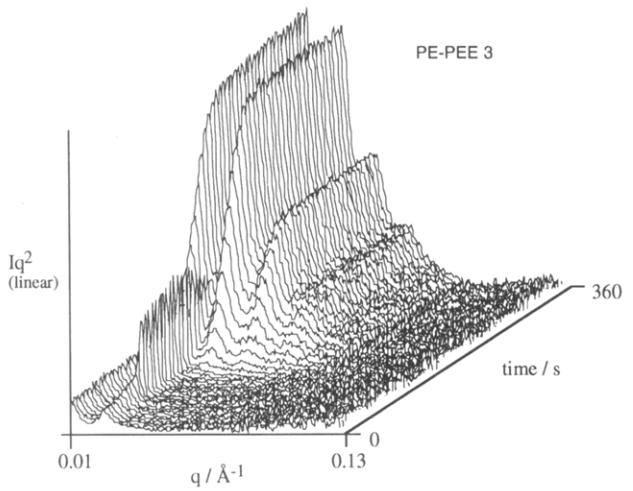

Figure 8. Time dependence of SAXS profiles for PE−PEE-3D during thermal treatment. The polymer was held at 140 °C until 648 s and then cooled at approximately 40 °C/min to 100 °C at 702 s. The data were collected at 6 sec/frame.

Typical time evolution of the WAXS data is presented in Figure 9, using the most crystalline PE−PEE-7H as an example. The (110) and (200) reflections from crystalline PE develop at the same rate after the discontinuous crystallization process.

The position of the most intense SAXS peak for PE−PEE-3D varies as a function of time following under-

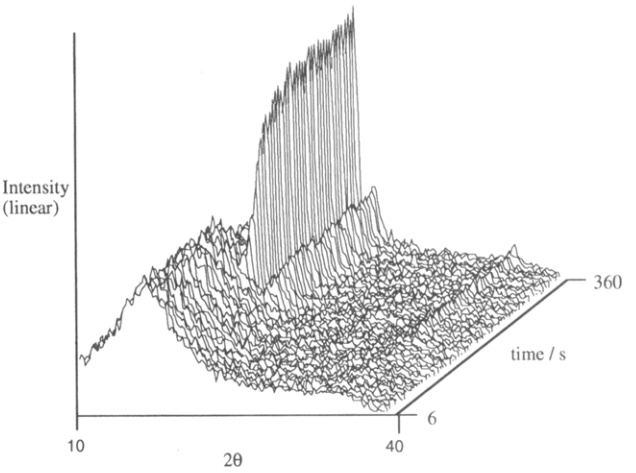

Figure 9. WAXS patterns over a temperature interval from 140 to 100 °C for PE−PEE-7H.

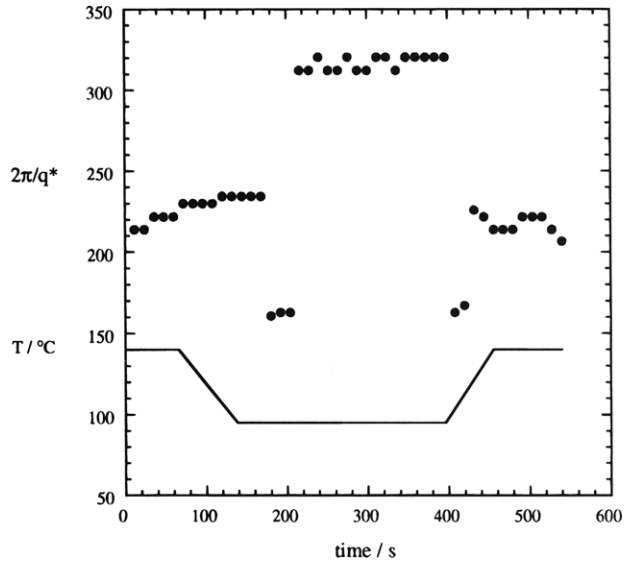

Figure 10. Position of the most intense peak for PE−PEE-3D on varying the temperature through the profile shown at the bottom.

cooling in an unusual manner as illustrated in Figure 10. The period corresponding to the correlation hole in the disordered melt increases as the temperature decreases because the chains stretch, as expected for our polyolefins.[15,30] During crystallization a continuous increase in the underlying PE pattern occurs so that the second-order crystal peak corresponding to $d = 160$ Å is most intense for 18 s before the first-order peak corresponding to $d_{sol} = 314$ Å becomes more intense. The same effect is observed on reheating. This shows that the lamellar structure is formed with PE crystallization driving the formation of a distinct new lamellar structure from the original cylindrical or lamellar morphology. In further experiments, we have found that this behavior is not qualitatively changed on varying the cooling rate.

The relative SAXS invariant Q' and the integrated (110) reflection intensity X are shown during a cooling and heating cycle for PE−PEE−3D in Figure 11. The coincidence between these measures of crystallinity is remarkable and illustrates that crystallization and the associated microstructure formation occur together.

Finally, the relative fraction of crystallized material, $(1 - \phi)$, determined from the SAXS invariant is shown on a double-logarithmic scale as a function of time (also

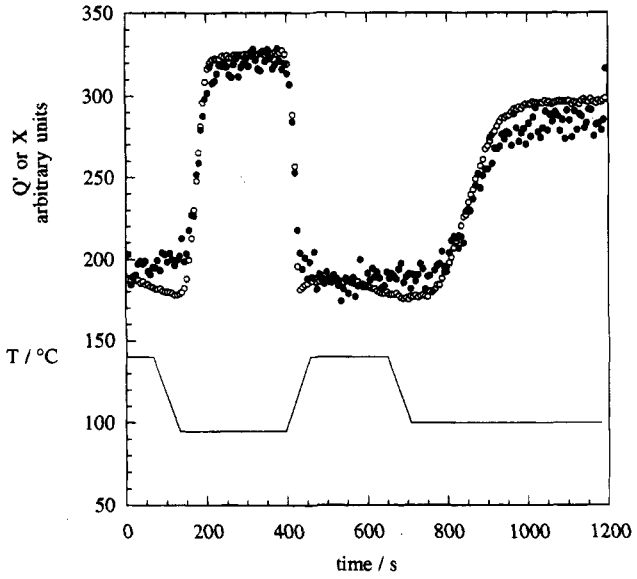

Figure 11. Temperature dependence of the SAXS invariant (Q, open symbols) and the integrated (110) reflection (X, filled symbols). The temperature profile used is also shown.

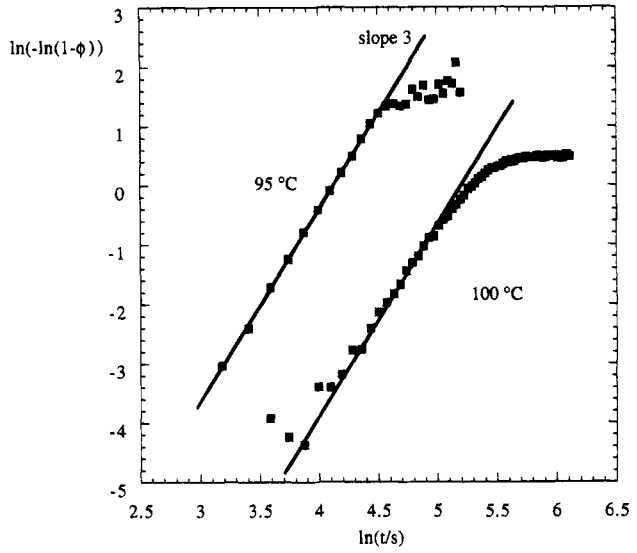

Figure 12. Avrami plots for the crystallization kinetics of PE–PEE-3D at 95 and 100 °C. The double logarithm of the relative degree of crystallinity ($1 - \phi$) determined from the SAXS invariant is plotted against the logarithm of the time.

on a logarithmic scale) for PE–PEE-3D in Figure 12. Using the Avrami-type equation

$$\phi = 1 - \exp(-kt^n) \quad (5)$$

where k is a rate constant, the slope of the linear portions gives the exponent n. For all the PE–PEE samples that we studied, we found $n = (3.0 \pm 0.1)$, which is characteristic of a nucleation and growth process such as the spherulitic growth of polymer lamellae.[31] This exponent was also found from the integrated (110) WAXS intensities, although this data is somewhat noisier.

Summary

We have studied structure development in poly(ethylene)-containing diblock copolymers crystallizing from the ordered melt using SAXS, WAXS, and DSC. Chain folding of poly(ethylene) in these samples destroys microphase-separated morphologies. A sample containing 49% PE formed a lamellar melt morphology; then on quenching below T_m a semicrystalline lamellar structure grew by a nucleation and growth mechanism. The domain spacing of the crystallized lamellar structure increased substantially compared to the melt to incorporate the chain-folded poly(ethylene). A 25% PE sample forming a hexagonal-packed cylinder phase in the melt transformed into a lamellar structure on crystallizing, showing that the free energy for chain folding on crystallization overwhelms the compositional enthalpy associated with the microphase-separated structure. The hexagonal-packed cylinder structure of a 75% PE structure was also destroyed by crystallization; however, we are not able unambiguously to identify the solid structure.

The SAXS profiles for the solid structures were shown to contain a contribution from semicrystalline poly(ethylene), giving a broad peak centered around $q \approx 0.05$ Å^{-1}, plus several orders of Bragg peaks from a regular lamellar structure. The profiles were further interpreted using density correlation functions calculated from the SAXS data. The degrees of crystallinity obtained are in reasonable agreement with those determined from DSC data, $X_{PE} = (0.4 \pm 0.1)$. The WAXS data show that PE crystallizes in its usual orthorhombic form for all samples.

These results for crystallization from the ordered melt may be contrasted with previous work on samples crystallized from the homogeneous melt. Rangarajan and co-workers found that segregation of poly(ethylene)-containing diblocks quenched from the homogeneous melt was not preceded by microphase separation in the melt.[14,32] Nojima et al. reached similar conclusions after time-resolved SAXS experiments on their diblocks with $T_{ODT} < T_m$.[13] We found that quenched PE–PEE-2D, which has $T_{ODT} < T_m$, crystallizes directly from the disordered melt. In contrast, Nojima et al. found transient Bragg peaks in the SAXS curves of quenched samples with $T_{ODT} \sim T_m$, indicative of an ordered melt structure.[13]

Crystallization and microstructural development were shown to occur in tandem, because the SAXS invariant and integrated WAXS (110) peak intensity show identical growth kinetics. The development of these quantities was fitted using Avrami equations, which show that crystallites develop in a nucleation and growth process. We will report in a forthcoming publication on the orientation of the PE unit cell with respect to the lamellae based on recent work on shear-oriented diblocks.

Acknowledgment. We are grateful to the Engineering and Physical Sciences Research Council (EPSRC) for funding and to NATO for a travel grant to I.W.H. F.S.B. received support from the National Science Foundation (NSF/DMR-9405101) for this work.

References and Notes

(1) Bates, F. S.; Fredrickson, G. H. *Annu. Rev. Phys. Chem.* **1990**, *41*, 525.
(2) Binder, K. *Adv. Polym. Sci.* **1994**, *112*, 181.
(3) Bates, F. S.; Schulz, M. F.; Khandpur, A. K.; Förster, S.; Rosedale, J. H.; Almdal, K.; Mortensen, K. *Faraday Discuss.* **1994**, in press.
(4) Hamley, I. W.; Koppi, K. A.; Rosedale, J. H.; Bates, F. S.; Almdal, K. A.; Mortensen, K. *Macromolecules* **1993**, *26*, 5959.
(5) Förster, S.; Khandpur, A. K.; Zhao, J.; Bates, F. S.; Hamley, I. W.; Ryan, A. J.; Bras, W. *Macromolecules* **1994**, *27*, 6922.

(6) Hajduk, D. A.; Harper, P. E.; Gruner, S. M.; Honeker, C. C.; Kim, G.; Thomas, E. L.; Fetters, L. J. *Macromolecules* **1994**, *27*, 4063.
(7) Leibler, L. *Macromolecules* **1980**, *16*, 1302.
(8) Helfand, E.; Wasserman, Z. R. In *Developments in Block Copolymers*; Goodman, I., Ed.; Applied Science: New York, 1982; Vol. 1.
(9) Cohen, R. E.; Cheng, P.-L.; Douzinas, K.; Kofinas, P.; Berney, C. V. *Macromolecules* **1990**, *23*, 324.
(10) Séguéla, R.; Prud'homme, J. *Polymer* **1989**, *30*, 1446.
(11) Douzinas, K. C.; Cohen, R. E. *Macromolecules* **1992**, *25*, 5030.
(12) Douzinas, K. C.; Cohen, R. E.; Halasa, A. F. *Macromolecules* **1991**, *24*, 4457.
(13) Nojima, S.; Kato, K.; Yamamoto, S.; Ashida, T. *Macromolecules* **1992**, *25*, 2237.
(14) Rangarajan, P.; Register, R. A.; Fetters, L. J. *Macromolecules* **1993**, *26*, 4640.
(15) Rosedale, J. H.; Bates, F. S.; Almdal, K.; Mortensen, K.; Wignall, G. D. *Macromolecules* **1995**, *28*, 1429.
(16) Young, R. N.; Quirk, R. P.; Fetters, L. J. *Adv. Polym. Sci.* **1984**, *56*, 1.
(17) Hamley, I. W.; Gehlsen, M. D.; Khandpur, A. K.; Koppi, K. A.; Rosedale, J. H.; Schulz, M. F.; Bates, F. S.; Almdal, K.; Mortensen, K. *J. Phys. (Fr.) II* **1994**, *4*, 2161.
(18) Zhao, J.; Schulz, M. F.; Majumdar, D.; Bates, F. S.; Almdal, K.; Mortensen, K.; Hajduk, D.; Gruner, S., to be submitted.
(19) Bras, W.; Derbyshire, G. E.; Ryan, A. J.; Mant, G. R.; Felton, R. A.; Lewis, R. A.; Hall, C. J.; Greaves, G. N. *Nucl. Instrum. Methods Phys. Res.* **1993**, *A326*, 587.
(20) Bras, W.; Derbyshire, G. E.; Cedie, J.; Komanschek, B. E.; Devine, A.; Clark, S. M.; Ryan, A. J. *J. Appl. Crystallogr.* **1995**, *28*, 26.
(21) Brandrup, J.; Immergut, E. H., Eds. *Polymer Handbook*, 3rd ed.; Wiley: New York, 1989.
(22) Koppi, K. A.; Tirrell, M.; Bates, F. S.; Almdal, K.; Mortensen, K. *J. Rheol.* **1994**, *38*, 999.
(23) Glatter, O. In *Small Angle X-ray Scattering*; Glatter, O., Kratky, O., Eds.; Academic: London, 1982; Chapter 4.
(24) Nye, T. M. W., unpublished results.
(25) Strobl, G. R.; Schneider, M. *J. Polym. Sci.* **1980**, *18*, 1343.
(26) Hamley, I. W.; Fairclough, J. P. A.; Ryan, A. J.; Towns-Andrews, E.; Bates, F. S., in preparation.
(27) Balta-Calleja, F. J.; Vonk, C. G. *X-ray Scattering of Synthetic Polymers*; Elsevier: London, 1989.
(28) Ryan, A. J.; Naylor, S.; Komanschek, B.; Bras, W.; Mant, G. R.; Derbyshire, G. E., *ACS Symp. Ser.* **1994**, in press.
(29) Stühn, B.; Vilesov, A.; Zachmann, H. G. *Macromolecules* **1994**, *27*, 3560.
(30) Almdal, K.; Rosedale, J. H.; Bates, F. S.; Wignall, G. D.; Fredrickson, G. H. *Phys. Rev. Lett.* **1990**, *65*, 1112.
(31) Sperling, L. H. *Introduction to Physical Polymer Science*, 2nd ed.; Wiley: New York, 1992.
(32) Rangarajan, P.; Register, R. A.; Adamson, D. H.; Fetters, L. J.; Bras, W.; Naylor, S.; Ryan, A. J. *Macromolecules* **1995**, *28*, 1422.

MA950023B